International Journal of Thermodynamics (IJoT)
ISSN 1301-9724 / e-ISSN 2146-1511
www.ijoticat.com

Vol. 22 (No. 4), pp. 184-191, 2019
doi: 10.5541/ijot.643311
Published online: December 01, 2019

Design and CFD Analysis of an Industrial Low-pressure Compressor for a Concentrating High-temperature Solar Power Plant

N. Cuturi[1], S. Aronica, L. Bellini, A. Salvati

La Sapienza, University of Rome
E-mail: cuturi.1646292@studenti.uniroma1.it[1]

Received 5 November 2019, Revised 19 November 2019, Accepted 22 November 2019

Abstract

The increasing need of renewable energy sources leads to the study of different alternative power plants. One of them is the thermo-electrical conversion by solar concentration power plants with an open volumetric receiver, using non-pressurized air as the heat transfer fluid. Due to the poor heat transfer characteristics, a large air mass flowrate is needed in the solar tower to transfer a sufficient amount of heat to a conventional steam power cycle. The subject of this study is a solar-thermal plant with 100 MW electrical power output. The intermediate heat transfer fluid, air, circulates in a semi-open circuit, and 1.125 compression ratio is required by the forced convection circuit. The inherently high air temperatures and mass flowrate require the design of a compressor from scratch, which is the aim of this study. The design starts from the selection and the sizing of the compressor, based on the standard mono-dimensional turbomachinery theory, and continue with the verification of its fluid dynamic performance, based on a commercial CFD code (ANSYS-FLUENT). A 2D case is evaluated first, to ensure that the geometry is working correctly, and then the full 3D geometry is simulated to quantify the real performance of the compressor. A preliminary structural analysis of the blade is also performed to verify the structural integrity of the chosen configuration.

Keywords: *Large low-pressure compressor; forced convection; concentrated solar power; CFD analysis; open volumetric air receiver; turbomachinery.*

1. Introduction

One of the concepts developed in the last decades in the field of concentrated solar energy conversion systems is the partial heat recovery obtained by recycling the air used as a primary heat transfer fluid (HTF), instead of using the more costly and technologically difficult molten salt solution. This technology presents remarkable advantages: non-pressurized air is freely available from the environment and is safer because its use avoids phase transitions problems. Air is chemically stable at high temperatures, in particular in the range considered by this solution [6], and this enables the system to reach higher thermodynamic efficiency, while the lower low heat capacity of the HTF allows for faster plant start up times [6]. A solar tower power plant essentially consists of a field of concentrating mirrors and of a final heat exchanger called "receiver" that collects the solar power and transfers it to the HTF: one of the most promising designs is the open volumetric air receiver (OVR). The main feature of the OVR is that the non-pressurized air is directly absorbed from the environment through the same area subjected to the radiation and is not confined in a close circuit as in the pressurized air plants, which results in a more efficient energy exchange [3]. As of today, several different designs of OVR have been developed, from porous ceramic materials to complex metallic structures with optimized heat transfer characteristics. In existing applications, the Concentrated Solar Powe rplant (CSP) with OVR is often associated with a heat recovery steam generator (HRSG) that transfers heat from the hot air to a conventional Rankine steam cycle. The plant layout consists in a heliostat field that concentrates solar energy on the receiver placed at the top of a tower, its height depending on the extension of the field and from the power generated. The air flowing through the receiver is heated to 650-700°C and feeds the HRSG through a recirculation system.

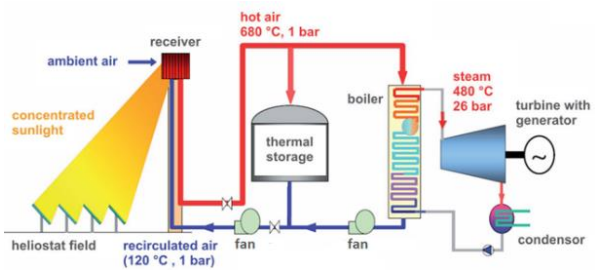

Figure 1. Schematic representation of common CSP layout [9].

One or more "blowers" move the cooled air exiting the HRSG through the circuit to the top of the tower where it is mixed with new hot air coming from the receiver (Figure 1): these machines are in fact low-pressure compressors that handle very large flowrate of a hot compressible fluid (the recirculated air). The early pioneering studies about open volumetric receivers began in north America in the late 1970 [5], but this system has not yet reached the technological level of its more conventional CSP competitors, although a 1.5 MW Solar Tower Jülich (STJ) pre-commercial OVR plant in Germany [6] was commissioned in 2009. This delay, as explained in detail in [5], is due to criticalities affecting the particular HTF used in these plants. The low heat

*Corresponding Author

capacity of air requires a high mass flow rate to be processed by the air recirculation loop. Furthermore, as stated by Romero [4], the heat transfer efficiency of the receiver is quite crucial and strictly related to the temperature of the returning air circuit. An efficiency near to 0.92 can be only achieved with an input temperature of 500°C. This forces the blower to operate on a low density medium that together with the high mass flow rate leads into an unexplored operational range for industrial turbomachinery. Furthermore, some OVR geometries may cause flow instabilities [5]. Besides causing dangerous local hot spots inside the receiver, they can also vary the fan outlet pressure causing overload or possibly off-design point operation with noticeable performance decrease. The intent of this study is to investigate these issues from a turbomachinery point of view. The preliminary design has been developed with the quasi mono-dimensional theory elaborated by Drzewiecki at the beginning of the 20th century [1], known as "finite blade elements", or more commonly as "velocity triangles method", which is still a reference today. To further investigate the initial geometry, we have used modern computational fluid dynamics techniques. First applied in 1968 to a NACA airfoil cascade with a Fortran routine by Katsanis [12], this approach has been developed parallel to the increase of computational power. In 1992, Osnaghi [11] presented a RANS solution approach to evaluate the three-dimensional flow in an axial fan. Since then, several eddy viscosity closures have been provided, the choice for this study being an advanced version of the k-ε standard method included in the CFD software ANSYS-FLUENT.

2. Design Process

2.1 Project Specification

This study is intended to provide a possible solution to the air circulation requirements. The plant taken in consideration is essentially an enlarged version of the 1.5 MW Solar Tower Jülich, studied and evaluated by Ertl [3]. it consists in a high temperature CSP with OVR that supplies heat together with a burner to a Rankine cycle for a total power of 100 MW. The blower considered here is one of the two installed in the plant, and in the following we shall refer to the main one which pushes the air directly to the top of the receiver tower. The operating conditions are reported in Table 1; the values of density and mass flow rate reflect the previous considerations.

Table 1. Design point conditions

Parameter	Unit	
Intake mass flow ($\dot{m}$)	[kg/s]	250
Intake air temperature	[°C]	200
Intake pressure	[bar]	0.910
Compression ratio	[-]	1.125
Isentropic efficiency	[-]	0,85

2.2. Preliminary Analytical Design

To focus on the correct type of turbomachine, it is necessary to investigate the possible occurrence of compressibility phenomenon. The increase in temperature experienced by the fluid in the polytropic compression is about 19° C, the corresponding increase of density is around 8%. In the literature [2], this amount of variation is considered as being the threshold between "blowers" and compressors. Therefore all the sizing is based on the similarity method related to the machine operating in a compressible environment (i.e., a compressor proper). The variation is small so the correction for the change in volumetric flow rate is operated not on the shroud diameter, that remains constant throughout the impeller, but on the flow coefficient (φ).

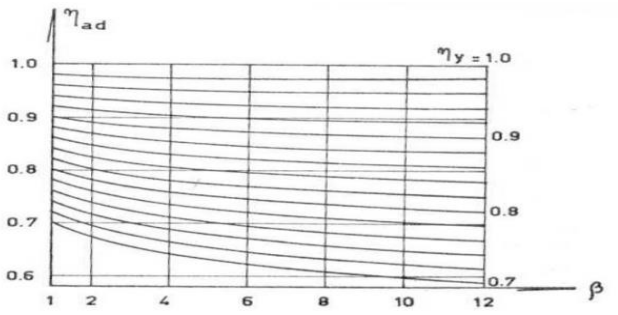

Figure 2. Relation between isentropic and polytropic efficiencies [8].

The isentropic stage efficiency is included in the specifications (Table 1) that correspond to a polytropic efficiency equal to 0.853 [8] (Figure 2). Based on the polytropic work it is possible to derive from Balje's charts the preliminary size for both an axial and radial configuration. The former has been preferred here because of it is more compact in size, considering that for centrifugal configuration the outside diameter would exceed 9 m. Assuming a tip speed of 300 m/s as the mechanical limit of this type of machine, the optimal set of Ns (2.2) and Ds (2) are selected in order to have the highest possible efficiency under the assigned specifications. This quasi-mono-dimensional study proceeds under the free vortex design assumption that posits that the streamlines at each span of the blade receive the same amount of energy, implying a zero radial velocity through the rotor. The shape of the rotor channel is also defined by the quasi-mono-dimensional theory. The hub-to-tip ratio (χ) is bounded below by the hub span deviation and above by the transonic limit at the tip span of the blade: the value selected here being $\chi = 0.67$. This value is also critical for the mechanical sizing of the blades because the main stresses are caused by centrifugal effects. The absolute flow deviation is corrected by the slip factor to account for the presence of viscid and inviscid phenomena that prevent the fluid to follow exactly the shape of the blade channels. The blade aspect ratio is evaluated from Eck charts with the values of the flow parameter and Ns [8]. Following an iterative process, blade solidity is chosen from the Howell charts in relation to the maximum possible deviation and this determines the number of rotor blades, $Z_b = 25$. The airfoil thickness is based on the NACA 0006 profile and, considering blade airfoil characteristics, NACA 63-206 was used as a reference to estimate a preliminary value for the incidence angle according to Cl/α and Cd/α polar diagrams. The stagger angle of the cascade is chosen in relation to the double arch nature of the camber line of the selected NACA airfoil and the deviation required. Table 2 reports the main results of this preliminary design. The degree of reaction is 0.83, which means that since the kinetic-to-pressure energy recovery downstream of the rotor is relatively small, it can be obtained by a correct design of the electric motor nacelle without the need for a proper bladed diffuser.

Table 2. Main parameter and values of the rotor geometry

	Unit		Span (0%)	Span (50%)	Span (100%)
Ns	[-]	2,2			
Ds	[-]	2			
T1	[K]	473°			
T2	[K]	492°			
Ls [8]	[J/kg]	19300			
P_1	[kg/m^3]	0.67			
D	[m]	3,28			
ω	[rad/s]	186,6			
χ	[-]	0,67			
Φ_1	[-]		0,46	0,37	0,31
Φ_2	[-]		0,43	0,34	0,29
Ψ_1	[-]		0,00	0,00	0,00
Ψ_2	[-]		0,46	0,30	0,21
α	[°]		5	4	3
γ	[°]		57,4	66,5	71,2
Rρ	[-]		0,80	0,89	0,93
Z_b	[-]	25			
σ	[-]		0.5	0.69	0.92

3. CFD Validation

3.1. Rotor Geometry

The rotor geometry has been digitalized using ANSYS-BLADEGEN, the software utility dedicated to turbomachinery topology of the Ansys commercial suite.

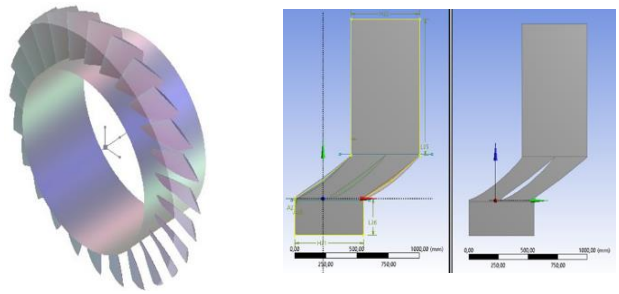

Figure 3. a) 3D view of the rotor geometry, b) the 2D fluid domain.

The CFD validation of the geometry starts with the simulation of the hub section 2D airfoil. According to the free vortex design, this location forces the highest flow deviation. Therefore, it is important to investigate whether the boundary layer wake can degenerate into stall conditions. A cascade of two rotor channels composes the 2D computational domain and it is extended by half a chord upstream and one chord downstream in order to properly apply the inlet and outflow boundary conditions (Figure 3).
The 3D geometry is composed by the fluid domain of one of the twenty-five blades, taking advantage of the radial symmetry to reduce the computational load. A shroud tip clearance of 0.8% is also added to the total blade span to investigate tip leakage phenomena. The 3D fluid domain is meshed by ANSYS-TURBOGRID, a mesh generator dedicated to turbomachinery topologies. Specific flags and sizing coefficients of the software govern the shape and dimensions of the elements in three areas of the domain: inflow, outflow and passage. Particular attention must be paid to the boundary layer parameter that influences directly the y+ of the solution.

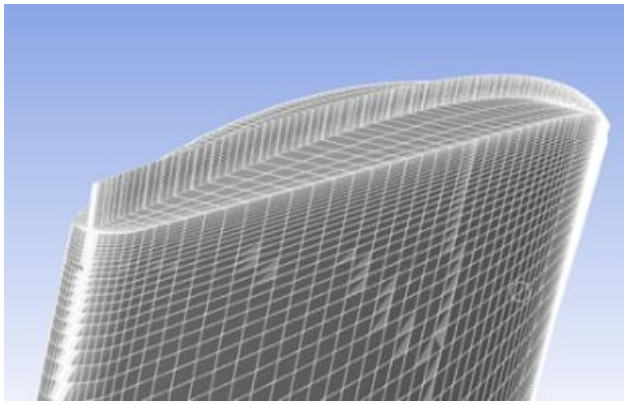

Figure 4. Shroud-tip interface.

3.2 Boundary Conditions and Numerical Set-up

The 2D domain identifies an inlet and outlet areas that are respectively set to pressure inlet and pressure outlet boundaries, as suggested by FLUENT, for compressible fluid solutions [7]. The lateral boundaries of the inlet and outlet blocks are set to translational periodic to respect the symmetry of the cascade. The turbulence model is k-ε standard with energy equation active to verify the effective change in temperature during compression. The solver is pressure-based and steady state, and works in the relative frame, which means that all the flow values are referred to velocities relative to the airfoil. This requires the fluid domain to be set with the translational velocity corresponding to the peripheral speed of the hub span. The fluid is treated as an ideal gas with an "operating pressure" [7] of 95000 Pa, which is the reference pressure of the CFD software and has been set to a mean of the expected values of the pressure field [7]. The segregation scheme for the solution is the SIMPLE type with second order precision for

the main solution variables. Appropriate under relaxation factors are chosen to stabilize the convergence. In order to achieve physically consistent results, the residuals for convergence are set to 10^{-6}. The solution is reached in about3000 iteration in a few minutes on a quad-core I7 processor.

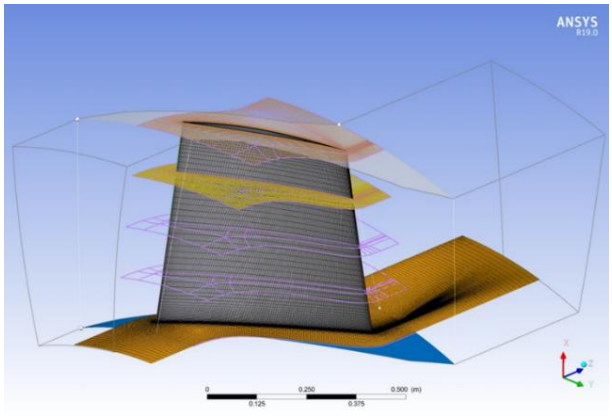

Figure 5. 3D fluid domain and mesh.

In the 3D case, Turbogrid slices automatically the domain in three cell-zones: inflow, outflow and passage. A rotation corresponding to the designed speed is applied to the zones, consistent with the absolute frame assumption (opposite to what was done in the 2D approach). Inlet and outlet areas are specified as pressure inlet and outlet, the radial boundaries are considered rotationally periodic. The shroud tip areas (Figure 4) created by Turbogrid are basically non-conforming surfaces and are regarded as "solid walls" by default in Fluent; in order to open the shroud tip clearance, they must be set as "interface" and then matched together to create an "interior" boundary. The turbulence model is still the k-ε standard with energy equation activated. In this case, the solver is pressure-based and set to steady state analysis, but the velocity formulation is absolute. The fluid is again an ideal gas with an "operating pressure" of 95000 Pa. The more advanced numerical parameters remain unchanged from the two-dimensional case. Due to insurgence of potential numerical instabilities the solution has been subdivided into several blocks of repeated iteration restarts, to reach the final convergence of the order of 10^5 in about 4000 iteration corresponding to few hours of operation of the same processor type.

3.3 Mesh Sensitivity and y+ Results

The analysis of results begins with the evaluation of the numerical parameters of the solution. For the two-dimensional analysis the mesh independence investigation shows a good insensitivity from 35000 elements with respect to the force acting on the airfoil (Figure 7). The maximum value of the y+ parameter is around 270 corresponding to the high turbulence area of trailing edge. On average 60 is a good value for the analysis of the boundary layer along the airfoil (Figure 6). Concerning the 3D solution, the quality of Turbogrid meshing algorithm provides a good mesh insensitivity of the physical parameters from 750000 elements (Figure 8a), in this case with respect to the blade torque on the axis. Figure 8b shows the y+ of the $1.5*10^6$ elements solution.

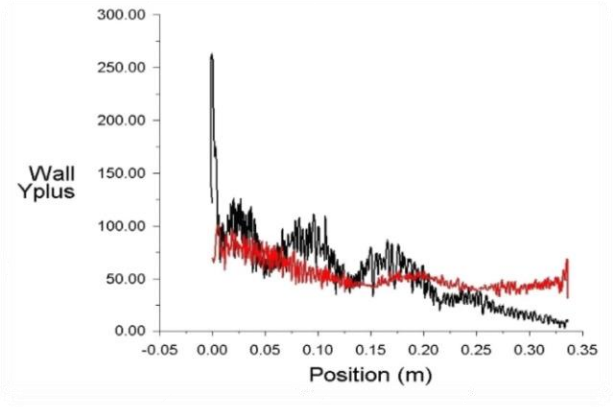

Figure 6. y+ plot of suction and pressure airfoil boundaries in the 2D analysis.

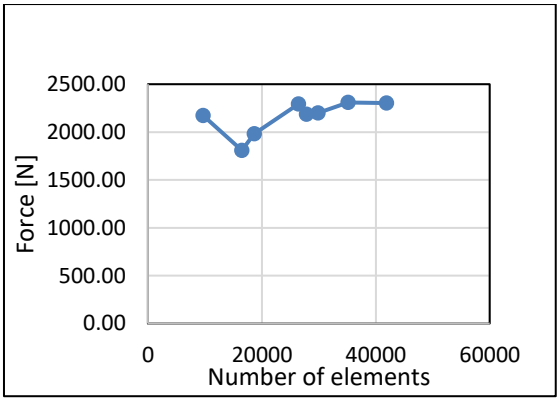

Figure 7. Mesh sensitivity plot of 2D analysis.

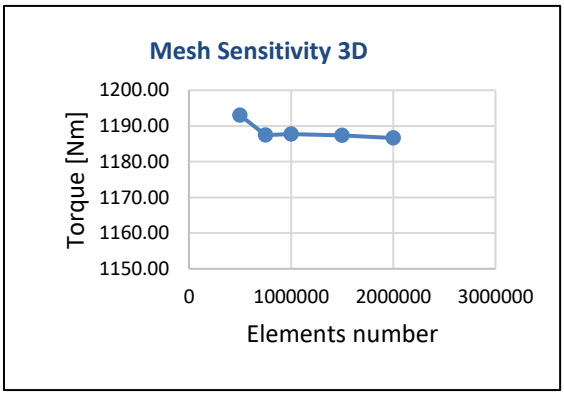

Figure 8a. Mesh sensitivity plot of 3D analysis.

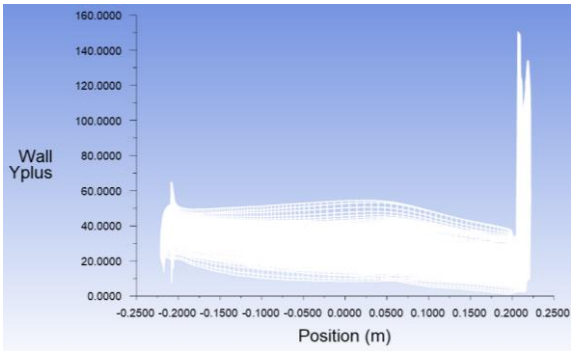

Figure 8b. y+ plot of 3D analysis.

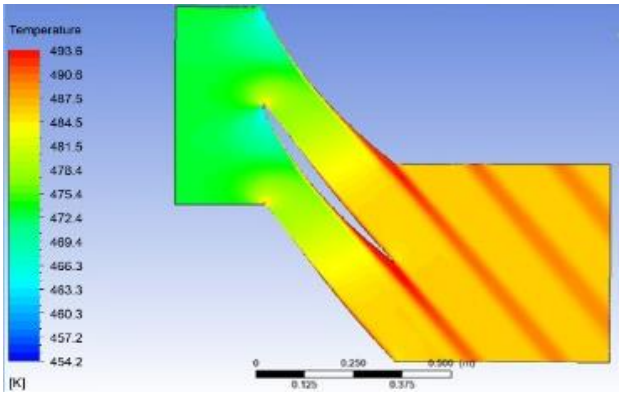

Figure 9a. Fluid domain contours: temperature distribution.

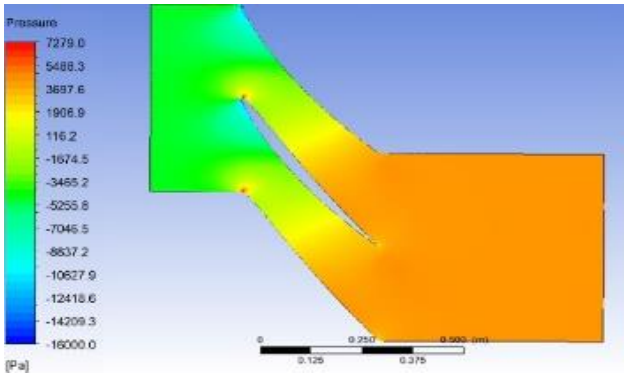

Figure 9b. Fluid domain contours: pressure distribution.

3.4 2D Results

The flow simulation for the hub span confirms that the airfoil geometry is working correctly and reaches the desired design point condition. The pressure distribution (Figure 9b) shows an overestimation of compressor performance of about 7% (with respect to the specified design values). The temperature contours (Figure 9a) confirm the presence of compressibility effects, showing an increase in temperature of 19° (average density variation of about 8%). The velocity distribution presents a wake of the boundary layer at the trailing edge that intensifies with the increase of incidence angle. Tests made with 3° and 5° degrees incidence showed a reduction of the turbulent kinetic energy at the trailing edge area (Figure 10). However, the compression ratio of the cascade is also reduced as a result of the lower lift generated. Thus an optimal range for cascade incidence can be identified between 3° and 5° degrees although the latter has been finally preferred for the hub span.

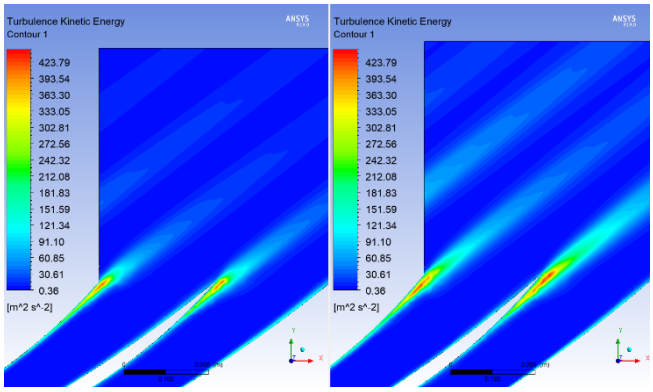

Figure 10. Kinetic turbulence distribution 3° (left) and 5°(right) incidence angle.

3.5 3D Results

The early simulations of the complete 3D domain showed numerical instabilities together with the inability to reach the desired performance (Figure 11b). A deeper investigation of the fluid behavior suggests a stall-like phenomenon identifiable at about the upper 50% span of the blade, which suggested to investigate more carefully the 2D flow over these sections.

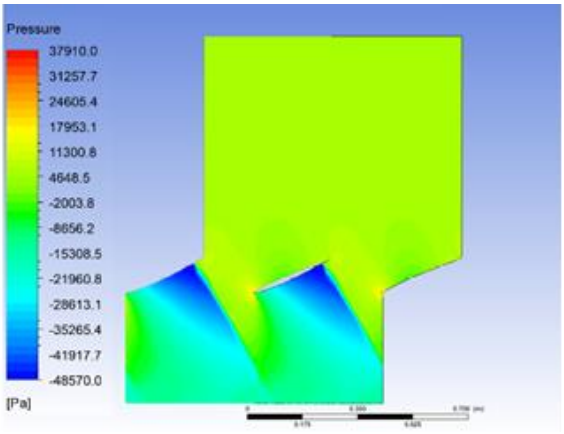

Figure 11a. 50% span blade channel with high pressure air infiltration.

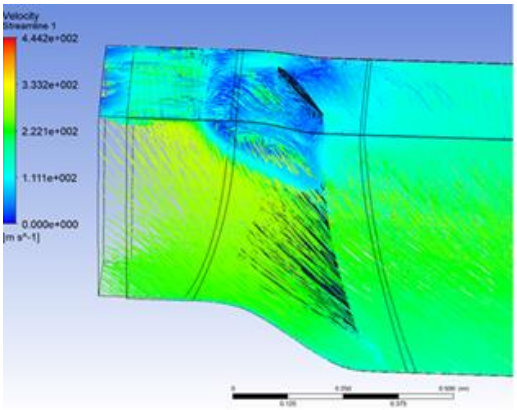

Figure 11b. Numerically instable solution with low solidity: streamlines.

Similarly to the hub span, the tip and mid one had been replicated for simulating two complete rotor channels. Contrary to the hub, the simulation of the other two span were demonstrating a large leak of high-pressure air towards the inlet section (Figure 11a) causing the stall of the blade cascade which under real operating conditions is likely to lead to compressor surge. The problem was solved by increasing the solidity of the tip and mid span with respect to the previous values chosen with the aid of the Howell charts. The tip and mid chord were lengthened of about 30% and 20% respectively.

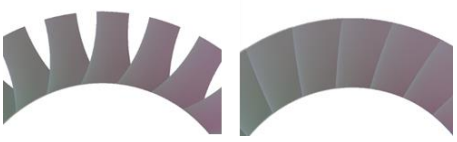

Figure 12. Solidity comparison between preliminary (left) and final configuration (right)

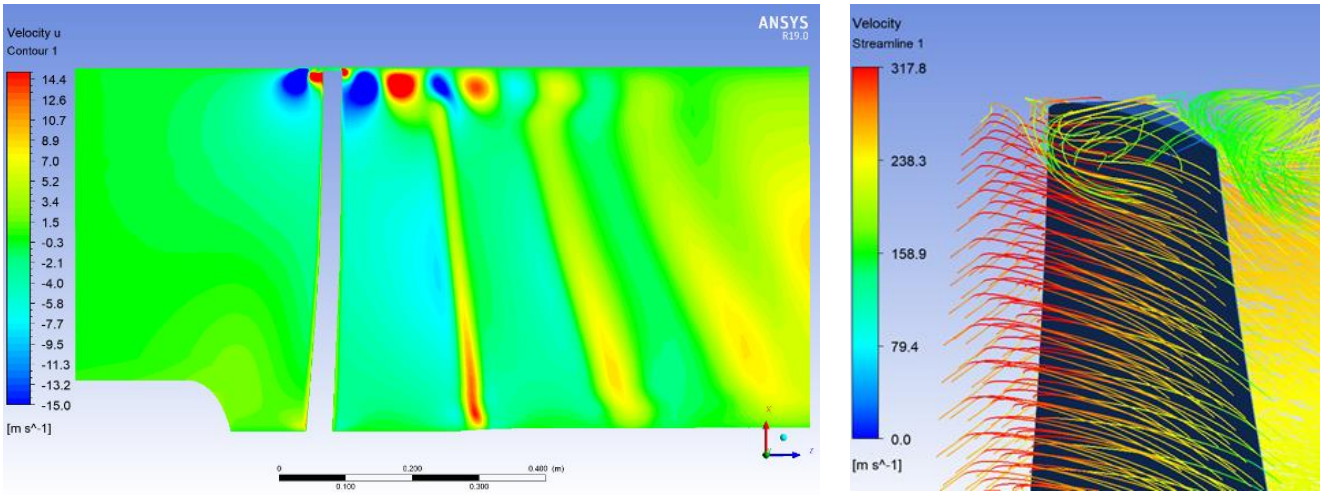

Figure 14. radial velocity contour plotted in a radial surface of the 3D domain (left), Tip-leakage streamlines (right).

The 3D simulations of the new geometry with augmented solidity show the performance predicted with the first 2D analysis. Overall, the 3D results are in excellent agreement with the 2D analysis, but comparing the hub sections, (Figure 9b and 13) it shows a slight reduction of performance, due to the presence of some secondary three-dimensional flows. It is possible to evaluate the correspondence of the results to the free-vortex oriented design in the radial velocity contour (Figure 14): the scale is set from -15 m/s to +15 m/s and the contours show a distribution of the velocity grouped around zero. In the upper portion of the passage it is possible to appreciate the radial velocities generated by the tip vortex, this is direct consequence of the tip-shroud clearance that generates the tip leakage losses.

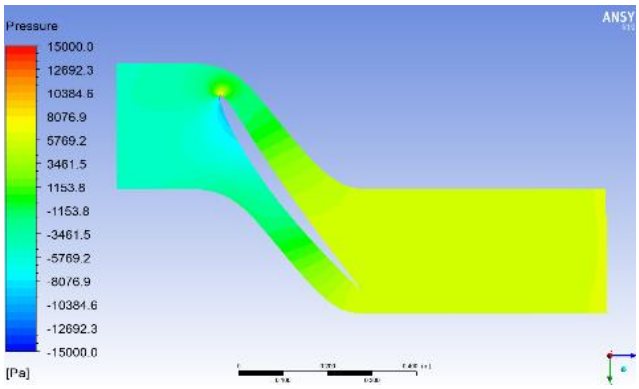

Figure 13. 50% span pressure contour of 3D domain.

The values extracted from the final converged 3D field led to the calculation of some significant performance parameters.

$$\eta_{cfd} = \frac{P_{pol}}{P_{cfd}} = 0.871 \quad (1)$$

$$\eta_{cfd} = \frac{\beta^{\frac{k-1}{k\eta_{pol}}} - 1}{\beta^{\frac{k-1}{k\eta_{pol.cfd}}} - 1} = 0.871 \quad (2)$$

$$P_{pol} = \dot{m} \cdot cp \cdot (T_2 - T_1) \quad (3)$$

$$P_{cfd} = N \cdot \omega \cdot T_q \quad (4)$$

Through Eqs. (3) and (4), it is possible to compute the polytropic power and the power evaluated in the CFD analysis via the predicted torque on the shaft, which are 4.835MW and 5.547MW respectively. Then with the result given by Eq. (1) it is possible to evaluate the CFD predicted polytropic efficiency by inverting the relationship in Eq. (2). The resulting value, 0.75, is in line with the current production standards of industrial machines

4. Preliminary Structural Analysis

Thanks to the multi-physical capabilities of ANSYS, it is possible to use the pressure distribution computed by the fluid dynamic analysis to perform a structural simulation. The study has considered both the aerodynamic and the centrifugal forces acting on each blade element. The constraint applied to the blade are a fixed bottom section and a rotational speed of 1856 rpm, equal to the design point speed. The structure is completely filled (no cavities within the blade), and the mesh is composed of 22118863 elements. The materials compared at this stage are an Aluminum alloy (density: 2800 Kg/m^3) and a generic structural steel (density: 7800 Kg/m^3). The comparison between the two material underlines how low density plays a fundamental role in limiting the centrifugal stresses: on average the steel blade experiences a stress of 650 MPa (Figure 15), the Aluminum one 225 MPa.

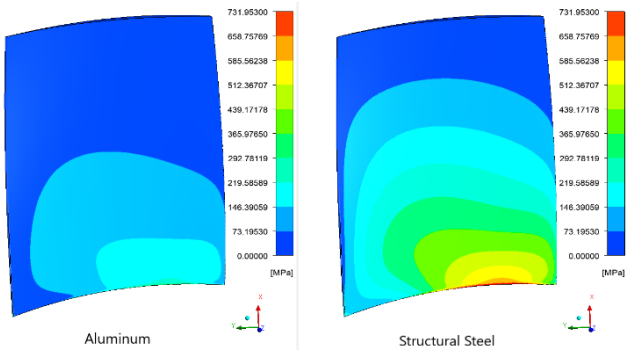

Figure 15. Contour of Von Mises equivalent stress.

The maximum deformations in the radial direction are quite similar for the two materials, resulting in 1.53 mm for the Aluminum and 1.44 mm for the steel (Figure 16). Thus, despite the high stress acting on the blade there are no interference problems with the shroud. From an operational

point of view, temperatures near 200°C cause a drop in the mechanical characteristics of most common high strength light alloys [10], like Ergal, determining the unfeasibility of aluminum solution for the present application. The results are consistent with rotating disc structural theory and identify the maximum stress area with the base section.

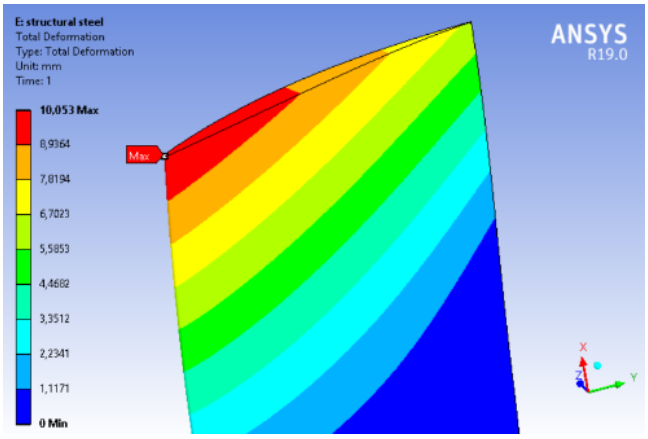

Figure 16a. Total deformation for the steel case.

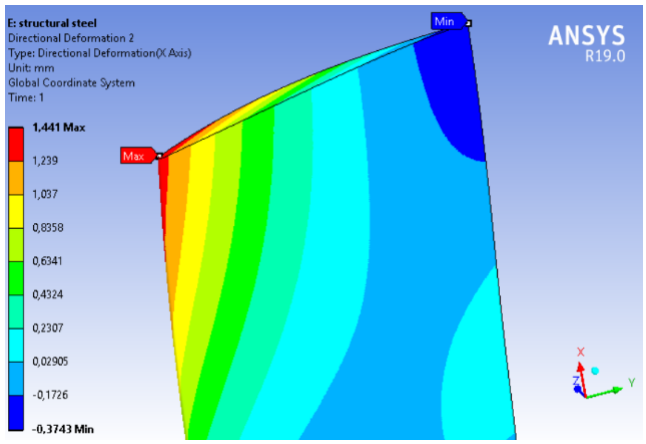

Figure 16b. Radial deformation for the steel case.

The structural simulation reveals that the edge of the blade base experiences the maximum stress; this behavior can be associated to the stress intensification factor caused by the sharp edge that it is possible to mitigate with a proper junction with the hub (Figure 17). No more detailed fluid/structure interaction analysis has been conducted in this study.

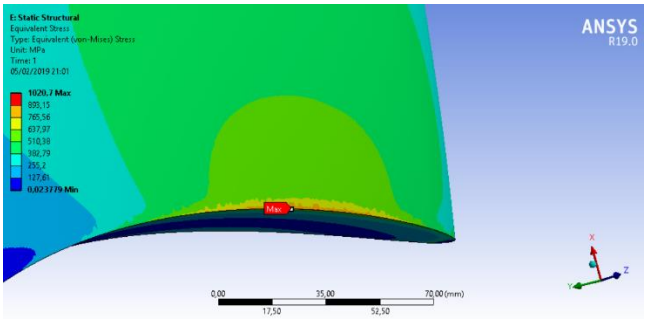

Figure 17. Sharp edge stress intensification.

5. Conclusions

This study presents a complete design process of a high-pressure axial fan (or, according to the current technical denominations, a low-p axial compressor) for the forced convection air circuit of OVR CSP power plants. Both the fluid dynamic and structural analysis have been developed using the commercial software ANSYS. The case studied represents the steady state operation at design point of the machine and highlights the main problems related to the environmental conditions and how they are reflected on the design choices. This study represents a valid design procedure in a new field of application for turbomachinery. It demonstrates the possibility to fulfill the process specifications completely. Therefore, it ought to be considered as a reference for future developments for this promising alternative to conventional energy conversion systems.

Nomenclature

Ns	=	Specific number of revolutions	
Ds	=	Specific diameter	
T1	=	Inlet temperature	K
T2	=	Outlet temperature	K
Ls [8]	=	Specific work	J
P_1	=	Inlet pressure	P
D	=	Rotor diameter	m
ω	=	Angular speed	rad/s
χ	=	Hub to tip ratio	
Φ_1	=	Inlet flow coefficient	
Φ_2	=	Outlet Flow coefficient	
Ψ_1	=	Inlet head coefficient	
Ψ_2	=	Outlet head coefficient	
α	=	Incidence angle	°
γ	=	Stagger angle	°
Rρ	=	Degree of reaction	
N	=	Number of revolutions	rpm
σ	=	Solidity	
k	=	Ratio of specific heat	
ß	=	Compression ratio	
cp	=	Constant pressure specific heat	J/KgK
η_{pol}	=	Ideal polytropic efficiency	
η_{cfd}	=	Predicted polytropic efficiency	
T_q	=	Blade torque	Nm
P_{pol}	=	Polytropic transform power	Mw
P_{cfd}	=	Predicted power	Mw
$\dot{m}$	=	Mass flow rate	kg/s

References

[1] Castegnaro S., Aerodynamic Design of Low-Speed Axial-Flow Fans: A Historical Overview. Designs 2, no. 3 (September 2018): 20.

[2] Culham R. G., Richard O., Scott R., Fans Reference Guide. 4th edition. Canada, 2001.

[3] Ertl F., Exergoeconomic Analysis and Benchmark of a Solar Power Tower with Open Air Receiver Technology, 2012.

[4] Marcos M. J., Romero M., and Palero S., Analysis of Air Return Alternatives for CRS-Type Open Volumetric Receiver. Energy, SolarPACES 2002, 29, no. 5 (1 April 2004): 677–86.

[5] de la Beaujardiere P., Jean-Francois P., Reuter H. C. R., A Review of Performance Modelling Studies Associated with Open Volumetric Receiver CSP Plant Technology. *Renewable and Sustainable Energy Reviews* 82 (1 February 2018): 3848–62.

[6] de la Beaujardiere P., Jean-Francois P., Reuter H. C. R., Sanford A. K., Reindl D. T., Impact of HRSG Characteristics on Open Volumetric Receiver CSP Plant Performance. *Solar Energy* 127 (1 April 2016): 159–74.

[7] Fluent User's Guide, ANSYS inc.

[8] Sciubba E., Lezioni Di Turbomacchine, Euroma, La Goliardica, Editrice Universitaria di Roma, 2001 (in Italian).

[9] Hirsch T., Ahlbrink N., Gall J., Nolte V., Teixeira Boura C. J., and Andersson J. A. E.. 'VICERP: Virtual Institute of Central Receiver Power Plants'.

[10] Senkova S., Senkov O., Miracle D., Cryogenic and elevated temperature strengths of an Al-Zn-Mg-Cu alloy modified with Sc and Zr. December 2006 Metallurgical and Materials Transactions A 37(12):3569-3575.

[11] Osnaghi, C. Prospettive Di Utilizzazione Delle Metodologie Di Calcolo Avanzato Nel Progetto Dei Ventilatori. Tecniche Avanzate Per Lo Studio Fluidodinamico Dei Ventilatori (Advanced Techniques for the Fluid-Dynamic Analysis of Fans); Seminar of the Associazione Termotecnica Italiana: Cagliari, Italy, 1992.

[12] Katsanis, T. Computer Program for Calculating Velocities and Streamlines on a Blade-to-Blade Stream Surface of Revolution; NASA Technical Note D-4525; NASA: Wayne, PA, USA, 1968.